Journal of Physics: Conference Series

PAPER • OPEN ACCESS

Impact of the rotor blades elasticity on the loads and wake of the large IEA 15-MW wind turbine

To cite this article: Francois Trigaux *et al* 2023 *J. Phys.: Conf. Ser.* **2505** 012034

Impact of the rotor blades elasticity on the loads and wake of the large IEA 15-MW wind turbine

Francois Trigaux[1], **Philippe Chatelain**[1], **Grégoire Winckelmans**[1]

[1] Institute of Mechanics, Materials and Civil Engineering (iMMC), Université catholique de Louvain (UCLouvain), 1348 Louvain-la-Neuve, Belgium

E-mail: `francois.trigaux@uclouvain.be`

Abstract. This work presents an investigation of the aeroelastic effects occurring on the IEA 15-MW reference wind turbine in a turbulent atmospheric boundary layer. Large Eddy simulation is carried out using an actuator line method coupled to the finite element beam solver *BeamDyn*. The results show that the blades experience significant displacements, leading to an important variation of the loads along the blade span. The turbulence also interacts with the blades natural frequencies, resulting in a variation of the spectra of the various loads. The impact of the flexibility is also evaluated on the wake by comparing the undeformed configuration with a statically and dynamically deformed rotor. It appears that the mean deformation plays an important role in the wake development due to changes in the load distribution, but that the dynamic effects have minimal impact on the wake behavior.

1. Introduction

Recent developments in wind energy have led to a rapid decrease of the levelized cost of energy. One of the primary factors contributing to this cost reduction is the increase in size of the wind turbines, which allows to enhance the rated power and the energy density of the wind farms. Nowadays, turbines with a rated power of 12 MW are commonly used in offshore conditions, and the industry is rapidly developing 15-18 MW prototypes with blades much longer than 100 m.

However, as the rotor diameter increases, fundamental changes of design are necessary to constrain the total mass of the blades to reduce the centrifugal and gravitational loads acting upon them. Therefore, recent blades are slender and made of lightweight composite materials, increasing their flexibility and potentially causing significant aeroelastic effects. The deformation of the blade structure modifies the aerodynamic behavior of the rotor by adding bending and twist. Additionally, the wind shear and turbulence create unsteady aeroelastic effects that can potentially lead to detrimental instabilities. To further reduce the cost of wind energy, gaining a more comprehensive understanding of the impact of aeroelasticity on large-scale wind turbines is required.

The objective of this study is to investigate the effects of the blade elasticity on a new generation offshore turbine, the IEA 15-MW [1], by quantifying the dynamic structural deformations under realistic operating conditions. The effect of these deformations on the blade loads and on the wake development is also assessed. To this purpose, Large Eddy Simulations (LES) of flexible wind turbines (represented using a flexible actuator line method (ALM), coupled with the structural solver *BeamDyn* from *OpenFAST*) are compared to their rigid counterparts in order to isolate the effects of the deformation.

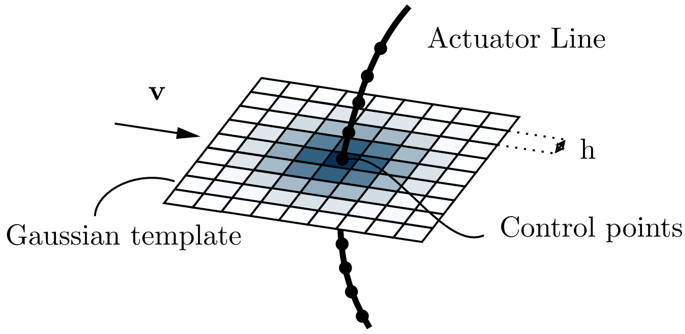

Figure 1. ALM with its associated template with Gaussian weights used for the effective velocity sampling and the forces distribution. Illustrated here for a Gaussian width of $\sigma/h = 2$.

Few studies use a similar methodology of coupling LES to a structural solver using an actuator method as interface. Storey *et al.* [2] coupled OpenFAST to an actuator disk method to perform simulations of one or two turbines and to compare their results to measurements. Vitsas *et al.* [3] used a modal structural model coupled to an actuator sector method to perform study of two wind farm configurations. More recently, OpenFAST was also coupled to Nalu-Wind and PALM [4, 5] to study the NREL-5 MW reference wind turbine. Hodgson *et al.* also performed validation of flexible actuator methods against high fidelity blade-resolved simulations, highlighting the ability of the ALM to accurately capture aeroelastic effect on rotors up to 5 MW [6, 7, 8]. Della Posta *et al.* also considered a two-way coupling between a structural solver and an ALM, including the tower, for unsteady aerodynamics of the NREL-5 MW rotor [9, 10]. However, all those studies consider medium-scale rotors with simpler structural parameters than the new generation turbines, which exhibit larger displacements and a more complex coupling between the degrees of freedom of the beam model. Moreover, the impact of the aeroelastic effects on the wake is not assessed.

This paper is structured as follows. The methodology is presented in Section 2, which describes the flow solver, the embedded flexible ALM and the coupling with the structural solver. Then, Section 3 presents a comparison between results obtained with our flexible ALM in uniform flow to those obtained using OpenFAST simulations, in order to verify the IEA 15-MW turbine model. The case of a wind turbine in realistic atmospheric conditions is then investigated in Section 4.

2. Methodology

2.1. Flow solver

The LES of turbulent flow is performed by solving the incompressible Navier-Stokes equations supplemented by a subgrid scale (SGS) model, using an in-house developed massively parallel code [11, 12]. The spatial discretization is achieved using fourth-order finite differences. The temporal integration is carried using a 2nd order Adams-Bashfort scheme (AB2). Energy preserving schemes are used to minimize spurious dissipation, which allows to accurately represent turbulent inflows and wakes. The Smagorinsky SGS model [13] is used, with the asymptotic value of $C_S = 0.027$ corresponding to LES where the grid size is much larger than the Kolmogorov scale [14]. It is supplemented by the wall model developed in [15] to handle the connection of the LES to the ground (here a ground with roughness). The turbulent inflow consists of a neutral atmospheric boundary layer obtained using a co-simulation [16]. The influence of the wind turbine on the flow is modeled using an actuator line method described hereunder.

2.2. Actuator Line Method (ALM)
The actuator line method (ALM) consists in representing the effect of the blades on the flow by adding a forcing term to the LES equations [17]. An advanced ALM is used, with 2D forces distribution and integral velocity sampling [18, 19]. The components of the aerodynamic force acting on each cross-section of the discretized blade are computed using the effective velocity sampled at the control point (corresponding to the aerodynamic center of the local airfoil profile) and the lift and drag coefficients of that airfoil. This effective velocity is obtained by interpolating the velocity at the flow solver grid points to the nodes of a 2D template centered on the control point and lying in the airfoil plane, as depicted on Figure 1. Then, the effective velocity is taken as a weighted average, using Gaussian weights. The distribution of the force is also performed in two steps. First, the force evaluated at the blade control point is distributed on the cells of the 2D template using the same Gaussian weights as that used for the velocity. Then, the force on each cell of the template is redistributed on the closest flow grid points using a linear distribution kernel (as this keeps the distribution as local as possible). Here, the position of the control points is also modified according to the structural deformation, so that the control points follow the deformed configuration.

For aeroelastic simulations, the accuracy of the loads provided by the ALM is essential as they drive the structural dynamics. However, this accuracy is often questioned, especially at the blade tip, mostly due to the regularization of the forces that reduces the induced velocity. To mitigate this issue, it is either possible to use tip corrections (see [20, 21, 22, 23]) or to use regularization kernels that lead to a more accurate prediction of the forces [24, 18]. The second approach is used here, by using the 2D Gaussian regularization for both the evaluation of the effective velocity. This leads to a better estimation of the aerodynamic loads, hence much decreasing the need for a tip correction, especially when slender blades are considered. A more detailed description of the used regularization is provided in Trigaux *et al.* [25] and its advantages over a 3D distribution are detailed in Caprace *et al.*.

2.3. Structural solver
The structural dynamics of the blades are simulated using the *BeamDyn* module from *OpenFAST* [26]. *BeamDyn* implements the nonlinear geometrically exact beam theory, which is particularly suited to study slender blades made of composite materials as it represents large displacements and allows the coupling of degrees of freedom using a full 6×6 cross-sectional mass and stiffness matrices. For the considered IEA 15-MW blade, this coupling mainly relates the flapwise and edgewise bending to the twist, which can substantially modify the angle of attack of the blade tip under classical loading conditions. The dynamic model provided in Gaertner *et al.* [1] is used, for which a preliminary analysis indicates that the time-step size must be constrained by $dt < 0.005$ seconds to correctly capture the first torsional mode. Each blade of the turbine is represented by one instance of the structural beam solver, for which the kinematics of the blade root is imposed based on the rotation speed. Thus, there is no coupling between the blades. This also allows to use a larger time-step for BeamDyn compared to an OpenFAST simulation, in which the structure-structure coupling between BeamDyn and ElastoDyn typically requires even smaller time increments. BeamDyn is coupled to the ALM as described in the following section.

2.4. Coupling
The coupling scheme linking the flow and structural solvers is the 2nd order Improved Serial Staggered (ISS) depicted in Figure 2 [27]. This scheme consists in evaluating the flow and the structural models at different time levels. The flow velocity is evaluated at time t and is used by the ALM to evaluate the aerodynamic forces based on the previous structural displacement $x(t - dt/2)$ and velocity $\dot{x}(t - dt/2)$. The structural solver then performs the time integration

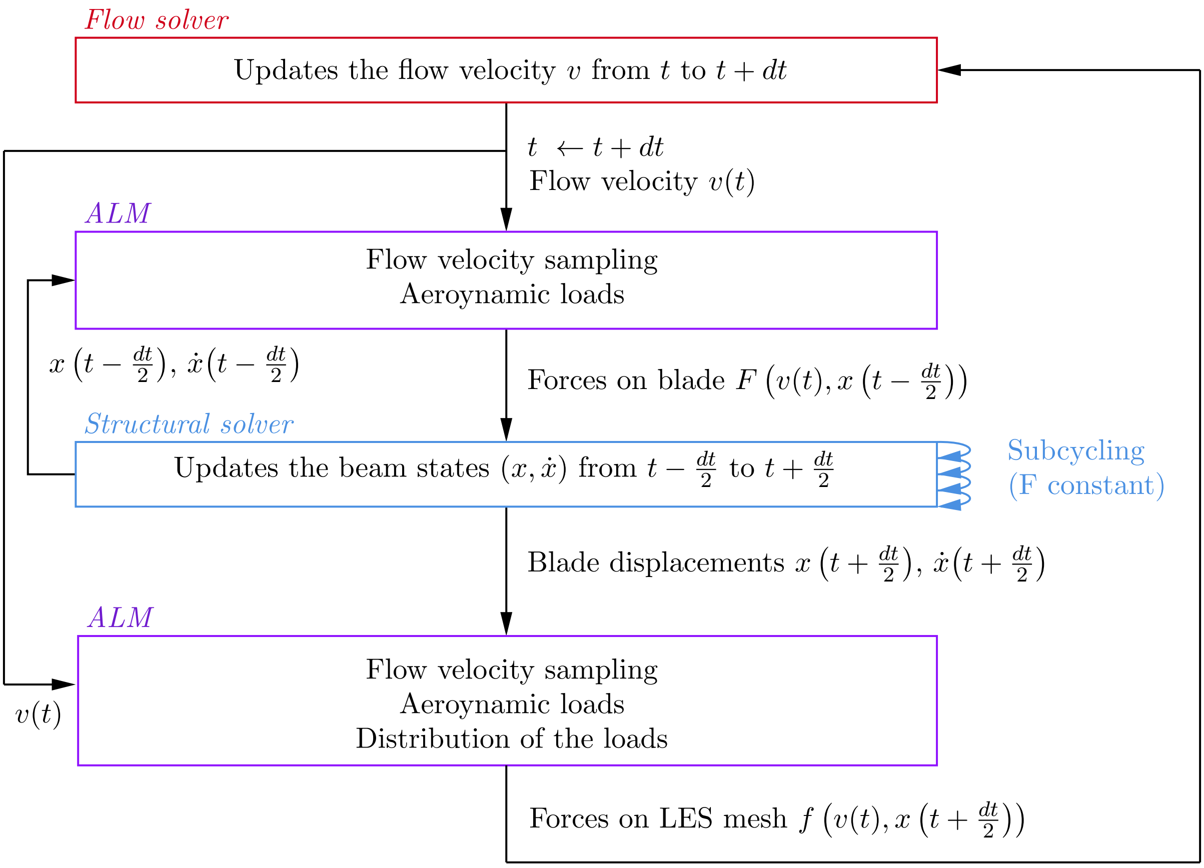

Figure 2. Schematic of the coupling between the flow and structural solver with the ALM as interface.

using sub-cycling (without reevaluation of the forces) in order to meet the structural solver requirements. Based on these updated states, the ALM computes the new forces and distributes them on the flow mesh according to the deformed configuration.

Using a serial coupling scheme requires that the flow solver waits for the results of the structural solver before proceeding to the time integration. Since the structural solver is here much faster to update than the flow solver, it does not imply a serious bottleneck in terms of computational time. For the simulations presented in the following sections, using the coupled method increased the total runtime by roughly 15%, which remains acceptable.

The presented methodology allows to simulate many rotations of wind turbines with flexible blades in LES at a reasonable computational cost. In what follows, it is applied to further investigate the implication of the flexibility on the IEA 15-MW reference wind turbine.

3. Comparison with OpenFAST

The methodology developed in the previous section is here tested and compared against the results obtained using OpenFAST. OpenFAST is an open source software based on engineering models to perform rapid simulations of wind turbines under various conditions [28]. It is widely used for design and analysis, and the presented comparison aims at verifying our methodology as well as pointing the limitations of some models.

The IEA 15-MW reference wind turbine is here considered with a uniform inflow. The blades have a length of 117 m and the hub radius is 3 m. To avoid tower strike, the blades are pre-bent

Table 1. Comparison of the time-averaged thrust coefficient(C_T), power coefficient (C_P) and tip deformation as predicted by the various methods.

Method		C_T [-]		C_P [-]		Flapwise [m]	Edgewise [m]	Torsion [deg]
Rigid	ALM	0.826		0.538		–	–	–
	OLAF	0.836	(+1.1%)	0.544	(+1.3%)	–	–	–
	BEM	0.804	(–2.7%)	0.488	(–9.2%)	–	–	–
Flexible	ALM	0.747		0.513		12.03	-1.04	-2.88
	OLAF	0.765	(+2.1%)	0.517	(+0.7%)	12.27	-1.08	-2.80
	BEM	0.732	(–1.8%)	0.479	(–6.3%)	11.76	-1.02	-2.83

by 4 m, the shaft is tilted by -6^o and the rotor has a cone angle of 4^o. For this case, the uniform wind speed is set to 9 m/s, which correspond to the second region of the controller, where the tip-speed ratio (TSR) is kept to its design value of 9. The gravity loads are also included. All the parameters used for this model are provided in the turbine definition, except from the structural torsional damping factor which was increased to avoid torsional instabilities when lift and drag coefficients from a steady state polar are used for the airfoil. The ALM and OpenFAST simulations are run for 200 seconds (which corresponds to $\simeq$ 21.5 rotations which is sufficient to reach steady state), and the results are averaged over the last four rotations. For the ALM simulations, the computational domain size is $8\,D \times 6\,D \times 6\,D$ (corresponding to the streamwise, vertical and transverse directions, respectively) with $D = 240$ m the turbine diameter. The turbine is located at a position $(3D, 3D, 3D)$ to ensure a sufficient distance from the domain boundaries. A uniform resolution of 64 flow grid points per diameter is used. For OpenFAST, two aerodynamic models are considered: the Blade-Element Momentum Theory (BEM) model and a free vortex wake model (cOnvecting LAgrangian Filaments, OLAF) [29, 30]. BeamDyn is used for the blade structural dynamics in all the considered cases. For the OLAF model, the time-step size is set to 0.155 seconds, which corresponds to an azimuthal increment $\Delta\theta \simeq 6^o$ per time-step, as suggested in the guidelines [30]. The circulation on the blade is obtained using the default C_l-based method. The near wake consists of 600 vortex panels, which gives a wake length corresponding to $\simeq$ 10 rotations. There is no far wake region. The last third of the wake is frozen to mitigate the effect of the wake truncation. The vortex core is regularized using the Vatistas vortex model with the optimized parameters option. The regularization also evolves with time using a viscous diffusion model (here with the parameter $\delta = 1000$). Interested readers can refer to the IEA 15-MW definition that contains an example case with OLAF [1].

A comparison of the rotor characteristics predicted by each method is provided in Table 1. For the rigid case, the thrust and power coefficients of the ALM and OLAF match well, whereas the BEM tends to predict a lower power coefficient. Those discrepancies are however reduced when flexibility is considered. At this operation point, the deflections of the blades is significant, especially in the flapwise direction. The additional torsion angle also importantly reduces the angle of attack near the tip, resulting in a noticeable variation of the thrust and power coefficients when accounting for the blade flexibility. Specifically, the thrust coefficient experiences a reduction of 10% whereas the power coefficient variation is closer to 5%

The aerodynamic forces acting on the rigid and flexible blade are displayed in Figure 3. For the rigid case, the forces obtained using OLAF and the LES using ALM match very well. The forces distribution predicted by the BEM is slightly lower in the flapwise direction and significantly lower in the edgewise direction. We can assume that LES/OLAF provide a better prediction given the higher fidelity level. We also recall that the BEM relies essentially on the

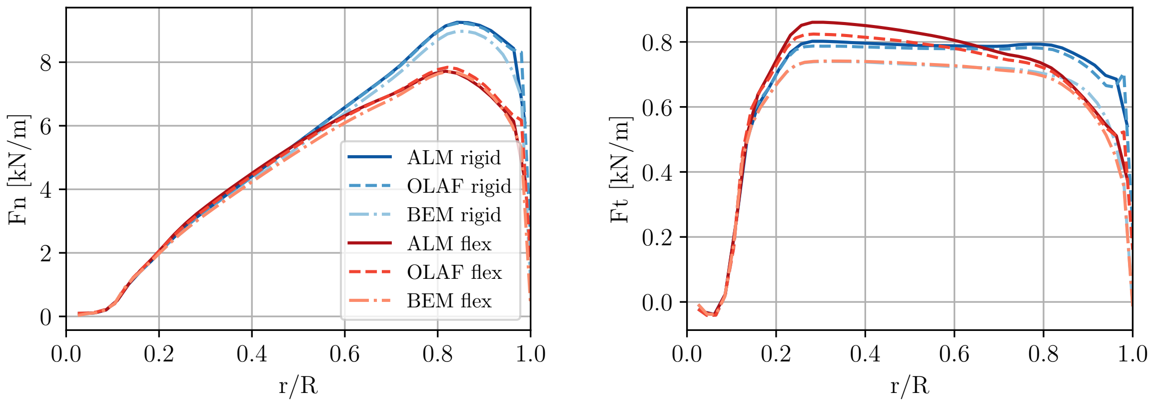

Figure 3. Steady state loads on the blades in the rigid (blue) and flexible (red) cases: ALM (dark solid), free vortex wake model OLAF (dash) and the BEM (light dash-dot) from OpenFAST.

empirical Glauert correction at this operation point, due to the high rotor loading.

When flexibility is considered, all methods predict a significant decrease of the loads on the outer part of the blade ($r/R > 0.6$). On the inner part of the blade ($r/R < 0.5$), OLAF and the ALM show an increase of the loads. This phenomenon arises from the additional flapwise deformation of the blade that modifies the location of the emission of the tip vortices and was also observed to a smaller extent for the NREL-5 MW turbine [31, 25]. It is not captured by the BEM as the effect of the blade curvature on its aerodynamics is not modeled [32]. In general, OLAF and the ALM also predict a much larger variation of the loads distribution between the rigid and the flexible rotors (especially in the edgewise direction). This highlights the importance of using higher fidelity methods when the aeroelasticity of large rotors is considered.

4. Investigation of rigid and flexible rotors in atmospheric conditions

In this section, rigid and flexible rotors are studied with a sheared turbulent wind as inflow, to evaluate the effects of the unsteady aeroelastic effects on the aerodynamic loads and on the wake. To that purpose, the numerical set up consists of a domain of size $8\,D \times 4\,D \times 4\,D$, again using 64 grid points per turbine diameter. The turbine location is $(3D, 150m, 2D)$. The time increment of the flow simulation is set so that the blade tip does not go through more than one grid cell per time-step. The inflow is generated using a co-simulation technique: first, the atmospheric boundary layer (ABL) is simulated until statistical convergence is reached; then, two simulations are run in parallel, the ABL simulation continuously feeding the wind turbine simulation with a realistic turbulent inflow. A neutral ABL (i.e., no buoyancy effects) is here obtained using a co-simulation [16], driven by a constant pressure gradient and using a roughness length $\epsilon = 0.0016$ m in order to obtain a velocity of $U_{hub} = 10$ m/s at hub height, with Turbulence Intensity (TI) of 6% .

Three cases are compared in this section. The first case is the "rigid undeformed" rotor, including the upwind pre-bend of the blades. The second case is the flexible rotor, modeled using the flexible ALM that dynamically deforms based on the aerodynamic loads. A third case considers a rigid rotor that includes the mean deformation of the blades, noted as the "rigid deformed" case. The deformed geometry was obtained by time-averaging the structural displacements obtained in the second case. This allows to isolate the effect of the time-varying response of the blade on the rotor dynamics and wake. In order to ensure a valid comparison of

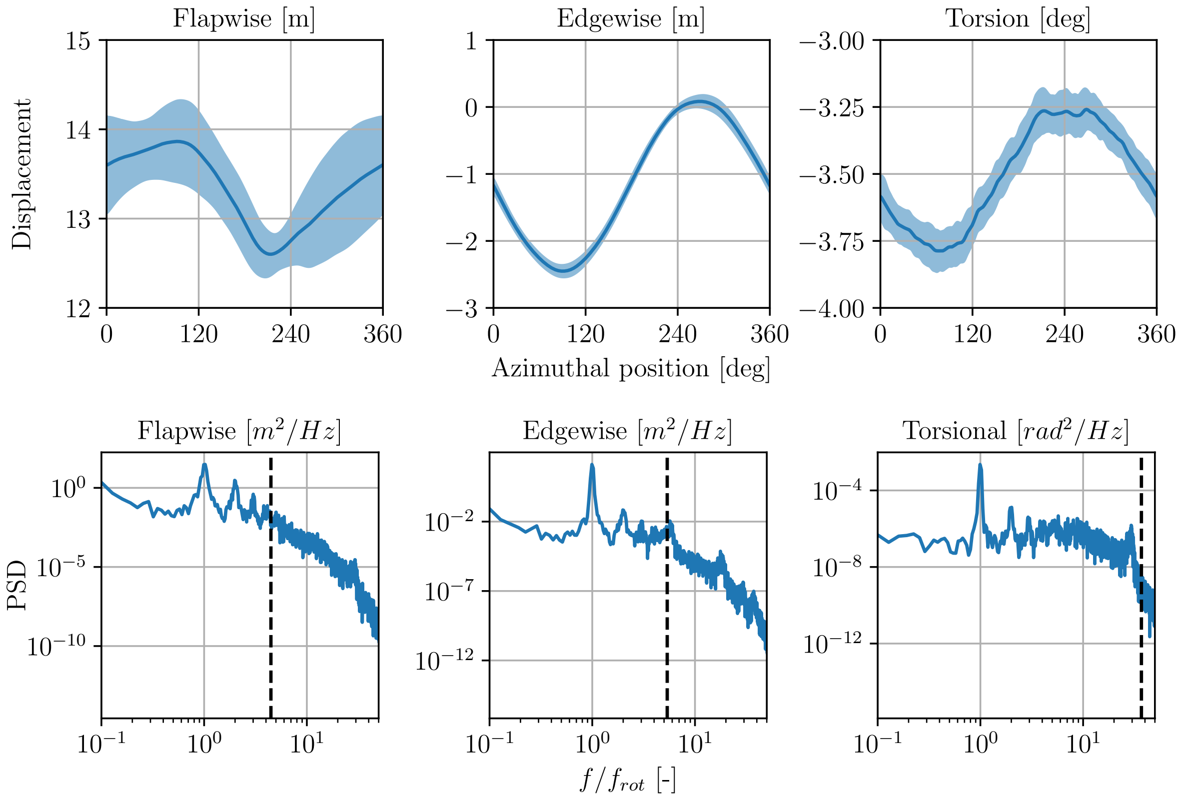

Figure 4. Time-averaged azimuthal mean (top) and PSD (bottom) of the blade tip displacement, computed over 100 rotations. The shaded area represents the standard deviation of each azimuthal position. The 0^o position corresponds to the blade pointing upward. The vertical dashed line indicates the first structural natural frequency for that direction.

the different parameters, all the turbines were set to a constant rotation speed corresponding to their design TSR (i.e., TSR = 9 based on the hub velocity).

The displacements of the blade tip and the excited frequencies obtained for the flexible rotor are first analyzed. Figure 4 depicts the time-averaged blade tip displacement over a rotation. The variation of the mean displacement over a rotation and the standard deviation remain moderate in all directions. In the flapwise direction, the displacement is minimal when the blade is pointing downwards, as the blade undergoes lower loads due to the lower velocity. The standard deviation is also minimal at this position. The displacement in the edgewise direction is mostly driven by gravity, and the deviation due to the aerodynamic loads is very limited. Interestingly, the mean torsional displacement has the same phase as in the edgewise direction, which could cause an imbalance between the left and right part of the rotor.

Figure 4 also displays the Power Spectral Density (PSD) of the tip displacement. The rotation frequency and its three first harmonics are clearly distinguishable in the spectra, indicating that the rotation is causing most of the displacement variations. In the edgewise direction, a peak is also observed at the natural frequency of the blade, which suggests that the unsteady aerodynamic loads interact with the blades at that frequency (see also [9]). For the twist displacement, the peak corresponding to the first mode appears below the natural frequency, due to the coupling with the aerodynamic loads which are a function of the angle of attack, itself influenced by the twist displacement.

The observed displacements are not without consequences for the loads acting on the blade.

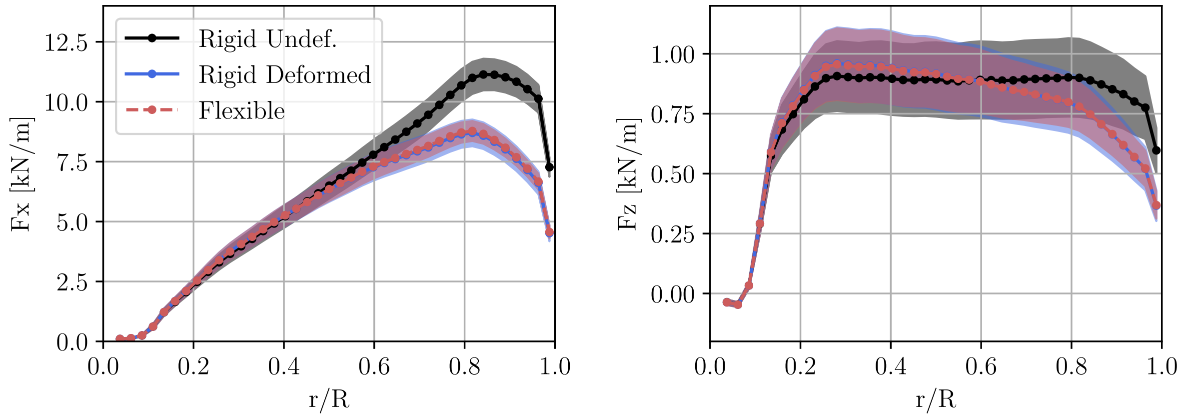

Figure 5. Distribution of the aerodynamic loads along the blade span for the rigid undeformed (black), rigid deformed (blue) and flexible (red) cases. The shaded area represents the standard deviation of the loads.

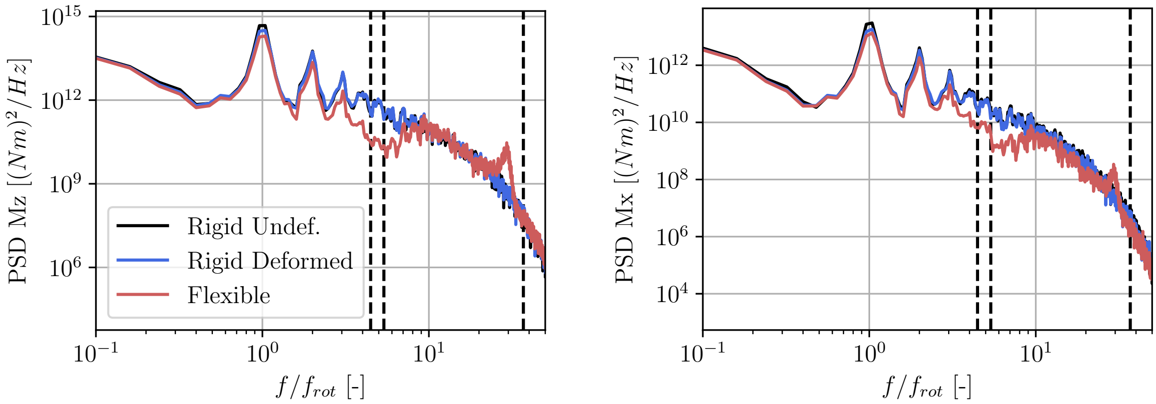

Figure 6. PSD of the moment of the aerodynamic forces on the blade root. Comparison between the rigid undeformed (black), rigid deformed (blue) and flexible (red) cases. The vertical lines indicate the blade natural frequencies of the first flapwise, edgewise and torsional modes.

A comparison of the mean load distribution is depicted on Figure 5, and exhibit noticeable differences between the rigid undeformed case and those that account for the deformation. In particular, a significant reduction of the mean loads and of their standard deviation is induced by the structural displacement on the outer part of the blade. This reduction of the standard deviation is also slightly more pronounced in the flexible case, due to the additional compliance of the blade.

Figure 6 presents the PSD of the moment of the aerodynamic forces on the blade root in the two directions. Although the rotation frequency is still important for each case, large differences appear close to the natural frequencies when the flexibility is considered. A substantial decrease of the PSD occurs close to the bending frequencies, due to the dynamic response of the blade. On the contrary, the root moments exhibit a noticeable increase at the torsional frequency due to the subsequent modification of the angle of attack of the blade. The modification of the spectrum of the root moment can have a direct impact on the lifetime of the turbine and the damage equivalent load calculations, as also obtained in [7]. Therefore, it is essential to consider dynamic models when assessing the structural integrity of the rotor.

The instantaneous out-of-plane vorticity field behind the rotor is depicted in Figure 7 on a

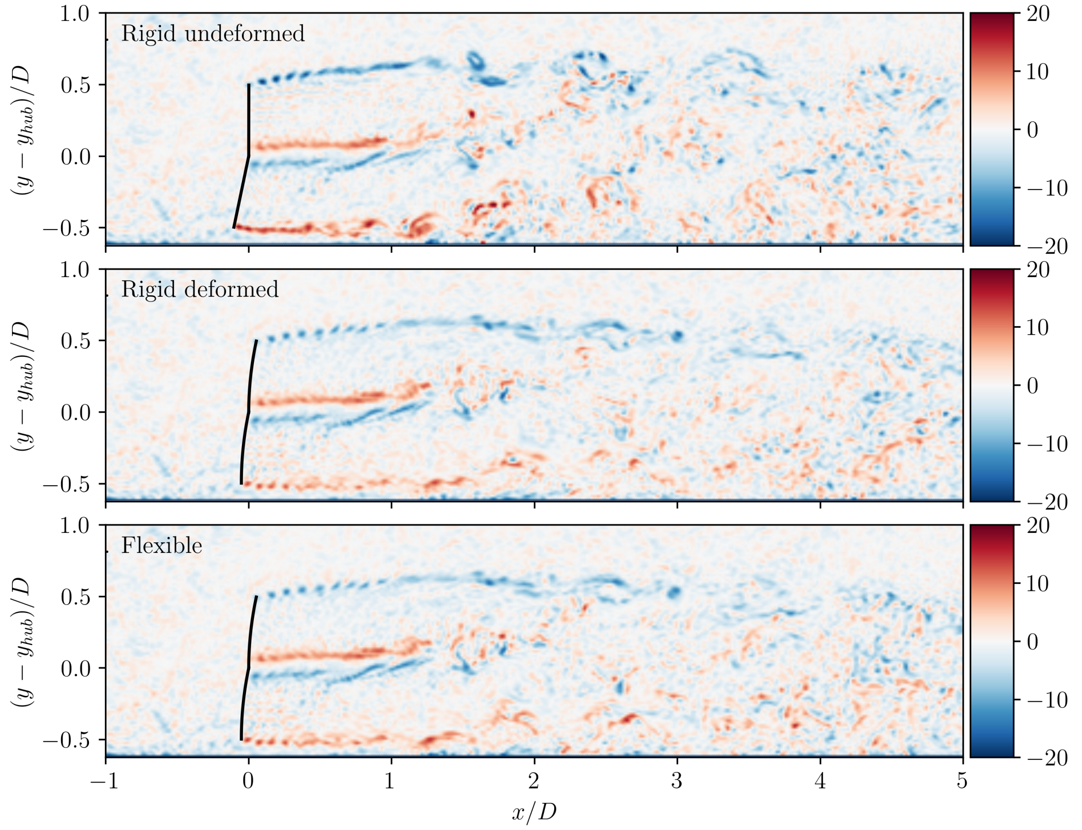

Figure 7. View of an instantaneous out-of-plane dimensionless vorticity ($\omega_z D/U_{hub}$) in the wake of the turbine for the rigid (top), deformed (middle) and flexible (bottom) cases. The inflow is identical for each case.

vertical plane. As a result of the blade displacement, the tip vortices are shifted downstream in the cases that include the deformation. In these cases, the destabilization of the wake also occurs further downstream due to the lower circulation of the shed vortices of the shed vortices. The rigid deformed and the flexible cases exhibit very similar vortical structures, suggesting that the unsteady variation of the displacements and forces play a minimal role in the wake dynamics.

The statistics of the wake are assessed for each case by comparing the time-averaged velocity deficit and the turbulent kinetic energy (TKE), as depicted in Figure 8 obtained by averaging the simulation over 50 turbine rotations. The mean velocity deficit behind the rigid rotor exhibits a stronger velocity gradient at the blade tip, which is consistent with the above-mentioned increase of the tip loading. The stronger individual vortices also logically lead to stronger variations of the velocity components and thence, to a higher TKE, and faster subsequent instabilities. The statistics of the rigid deformed and flexible cases are very similar, confirming the low impact of the unsteady aeroelastic effects on the wake development.

5. Conclusions

This work presents aeroelastic simulations of the IEA 15-MW reference wind turbine using a coupling between a flexible actuator line method in a LES flow solver, and the structural solver *BeamDyn*. This methodology leverages the LES capabilities to model the unsteadiness of the inflow (using a co-simulation of the ABL) and of the wake. The turbine is simulated over many rotations in order to properly quantify the structural displacements, the variation of the loads and their effects on the wake.

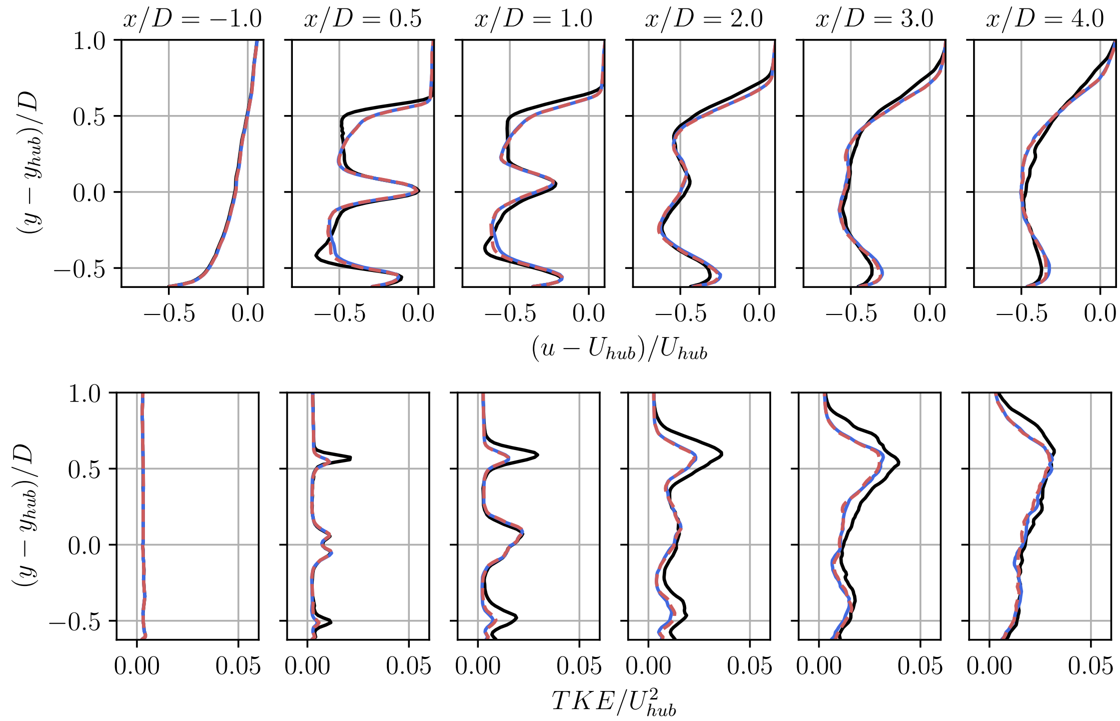

Figure 8. Profiles of mean velocity deficit (top) and turbulent kinetic energy (bottom) in the near wake of the turbine at various downstream locations: rigid undeformed (solid black), rigid deformed (solid blue) and flexible (dash red) cases.

In uniform flow, good agreement is found with *OpenFAST*, especially when the higher fidelity model OLAF is used for the aerodynamic part. It is also shown that the BEM model tends to predict a lower effect of the flexibility on the load distribution, especially in the edgewise direction. This arises from the fact that the BEM does not include the effect of the blade curvature on the wake. It emphasizes the need to use higher fidelity aerodynamic models when assessing the effect of the flexibility on the blade loads.

The IEA 15-MW reference wind turbine is then studied in a turbulent atmospheric boundary layer, generated using a co-simulation. The results show that the blades undergo substantial flapwise and torsional displacements that vary along the rotation due the mean sheared flow. The blade natural frequencies also appear to be excited by the turbulence. These displacement frequencies impact the blade root moment, which could potentially affect the lifetime of the blades. Finally, a comparison of the wakes reveals that it is necessary to include the mean deformation of the blade in order to accurately capture the wake dissipation; it also shows that the unsteady variations around the mean have little impact on the wake dynamics.

The present study mainly focuses on relatively steady operating conditions. However, the methodology has the ability to represent transient scenarios where the unsteady effects could have a more determining role. A potential additional source of unsteadiness is the control system of the turbine that modifies the rotation speed and the pitch angle, especially if individual pitch control (IPC) is considered. The flow can also exhibit larger unsteadiness when there is increased turbulence, such as in gust encounters and wake impingement situations. To better understand the impact of the aeroelasticity in these conditions, future work will investigate cases with higher levels of unsteadiness. Further comparisons with OpenFAST in unsteady conditions are also envisioned.

Acknowledgments
This research was funded by the Belgian Federal Government under the Energy Transition Fund in the frame of the PhairywinD project. It benefited from computational resources made available on the Tier-1 supercomputer of the Fédération Wallonie-Bruxelles, infrastructure funded by the Walloon Region under the grant agreement n°1117545. Computational resources have been provided by the supercomputing facilities of the Université catholique de Louvain (CISM/UCL) and the Consortium des Équipements de Calcul Intensif en Fédération Wallonie Bruxelles (CÉCI) funded by the Fond de la Recherche Scientifique de Belgique (F.R.S.-FNRS) under convention 2.5020.11 and by the Walloon Region

References

[1] Gaertner E, Rinker J, Sethuraman L, Zahle F, Anderson B, Barter G E, Abbas N J, Meng F, Bortolotti P, Skrzypinski W *et al.* 2020 Iea wind tcp task 37: definition of the iea 15-megawatt offshore reference wind turbine Tech. rep. National Renewable Energy Lab.(NREL), Golden, CO (United States)
[2] Storey R, Norris S, Stol K and Cater J 2013 *Wind Energy* **16** 845–864
[3] Vitsas A and Meyers J 2016 *Journal of Physics: Conference Series* **753** 082020 ISSN 1742-6596
[4] Sprague M A, Ananthan S, Vijayakumar G and Robinson M 2020 *Journal of Physics: Conference Series* **1452** 012071
[5] Krüger S, Steinfeld G, Kraft M and Lukassen L J 2022 *Wind Energy Science* **7** 323–344
[6] Sørensen J N, Mikkelsen R F, Henningson D S, Ivanell S, Sarmast S and Andersen S J 2015 *Philosophical Transactions of the Royal Society A: Mathematical, Physical and Engineering Sciences* **373** 20140071
[7] Hodgson E, Andersen S, Troldborg N, Forsting A M, Mikkelsen R and Sørensen J 2021 *Journal of Physics: Conference Series* **1934** 012014
[8] Hodgson E L, Grinderslev C, Forsting A R M, Troldborg N, Sørensen N N, Sørensen J N and Andersen S J 2022 *Frontiers in Energy Research* **10** 864645
[9] Della Posta G, Leonardi S and Bernardini M 2022 *Renewable Energy* **190** 971–992
[10] Della Posta G, Leonardi S and Bernardini M 2023 *Wind Energy* **26** 98–125
[11] Duponcheel M, Bricteux L, Manconi M, Winckelmans G and Bartosiewicz Y 2014 *International Journal of Heat and Mass Transfer* **75** 470 – 482
[12] Moens M, Duponcheel M, Winckelmans G and Chatelain P 2018 *Wind Energy* **21** 766–782
[13] Smagorinsky J 1963 *Monthly Weather Review* **91** 99–164
[14] Meneveau C and Lund T S 1997 *Physics of fluids* **9** 3932–3934
[15] Thiry O 2017 Investigation of wall shear stress models for large eddy simulation phD thesis at Université Catholique de Louvain
[16] Moens M 2018 Large eddy simulation of wind farm flows: improved actuator disk model and investigation of wake phenomena phD thesis at Université Catholique de Louvain
[17] Sorensen J and Shen W 2002 *ASME. J. Fluids Eng.* 393—399
[18] Jha P K and Schmitz S 2018 *Journal of Fluid Mechanics*
[19] Churchfield M J, Schreck S J, Martinez L A, Meneveau C and Spalart P R 2017 *35th Wind Energy Symposium* 1998
[20] Dağ K O and Sørensen J N 2020 *Wind Energy* **23** 148–160
[21] Meyer Forsting A, Pirrung G and Ramos-García N 2019 *Wind Energy Science Discussions* 1–22
[22] Martínez-Tossas L A and Meneveau C 2019 *Journal of Fluid Mechanics* **863** 269–292 ISSN 1469-7645
[23] Kleine V G, Hanifi A and Henningson D S 2022 *arXiv preprint arXiv:2206.05448*
[24] Caprace D G, Chatelain P and Winckelmans G 2019 *AIAA Journal* **57** 17–28
[25] Trigaux F, Chatelain P and Winckelmans G 2022 *Journal of Physics: Conference Series* **2265** 022050
[26] Wang Q, Sprague M A, Jonkman J, Johnson N and Jonkman B 2017 *Wind Energy* **20** 1439–1462
[27] Degroote J 2013 *Archives of computational methods in engineering* **20** 185–238
[28] Jonkman J 2013 The new modularization framework for the fast wind turbine cae tool *51st AIAA aerospace sciences meeting including the new horizons forum and aerospace exposition* p 202
[29] Jonkman J M, Hayman G, Jonkman B, Damiani R and Murray R 2015 *NREL Draft Report* 46
[30] Shaler K, Branlard E and Platt A 2020 Olaf user's guide and theory manual Tech. rep. National Renewable Energy Lab.(NREL), Golden, CO (United States)
[31] Dose B, Rahimi H, Herráez I, Stoevesandt B and Peinke J 2018 *Renewable Energy* **129** 591–605 ISSN 0960-1481
[32] Fritz E K, Ferreira C and Boorsma K 2022 *Wind Energy* **25** 1977–1994